

Polarization-Selective Fano-Resonance in Cascaded Frequency-Selective Surfaces

Deisy F. Mamedes and Jens Bornmann

University of Victoria, Victoria, BC, V8W 2Y2, Canada, (mamedes@ieee.org, j.bornemann@ieee.org)

Abstract—In this work we investigate a cascaded system of two symmetric frequency-selective surfaces (FSSs) that supports a Fano resonance (FR) at off-normal incidence in the millimeter-wave range. The first FSS is shaped with the four-arms star, and the second FSS is based on the quasi-square geometry. These two single-layer FSSs present resonant frequencies at 28 GHz (FSS #1) and 36 GHz (FSS #2). Cascading of the two FSSs was realized by using an air gap of 2.5 mm. The FSS prototypes were fabricated and measured in an anechoic chamber. It is demonstrated that a single FR is excited when the symmetry of the overall cascaded element is broken at an incidence of $\theta \geq 20^\circ$.

I. INTRODUCTION

Frequency-selective surfaces (FSSs) are two-dimensional arrays of periodic structures, formed by patch or aperture elements etched on a dielectric substrate, providing filtering properties of the incident electromagnetic waves [1], [2]. FSSs have been used in a wide range of applications from microwave to terahertz frequencies, such as in antenna radomes [3], reconfigurable antennas [4], polarization converters [5], radar cross-section reduction [6], and sensors [7]. The FSS frequency response depends on the thickness and electromagnetic characteristics of the dielectric material, the polarization and angle of the incident wave, and periodicity and geometry of the elements. The type of the element (patch or aperture) and its shape defines if the FSS has a capacitive or inductive response, i.e., the FSS presents an extended or narrow bandwidth, and suppression or promotion of grating lobes. In some designs, symmetrical-shaped elements are used to provide polarization stability. However, the symmetry of the element can be broken, exciting a Fano resonance (FR) [8], [9].

FR is an interference effect between two resonators. The resonances of these resonators are generally classified as bright (or continuum or broad) mode and dark (or discrete or narrow) mode [10]. The Fano effect arises when the geometry is broken, then the incident wave efficiently excites the bright mode, overlapping the dark mode, which does not couple efficiently to the wave. This scattering phenomenon is identified by nonlinear distortion of the transmission coefficient with ultrahigh quality factor (Q-factor) shifted from the central frequency [11]. The FR has been intensively studied in the fields of plasmonics and metamaterials [12]. Due to its unique sensitivity and high Q-factor, FR has found applications in ultrasensitive sensors [13], lasing [14], switching [15], slow light [16], and ultracompact antennas [17].

In this paper, we propose a cascaded FSS, consisting of two single-layer FSSs with different geometries, which can

generate a FR mode at oblique incidence in the millimeter-wave range. The numerical and experimental results prove that the FR is sensitive to the geometric parameters of the proposed FSS and polarization of the incident field.

II. DESIGN

This section presents the design of two individual geometries, followed by the combination of these two layers to achieve the cascaded FSS. The numerical characterizations of all structures are obtained through the commercial software package CST Microwave Studio.

A. FSS #1

The first FSS (FSS #1) is based on the four-arms star whose geometry of the unit cell including its parameters are illustrated in Fig. 1a. Initially, the unit cell dimension is defined as p , and then a rectangular patch is designed as a , where the arms are shaped. From the edges, lines cross the rectangular patch with b , and the four-arms star geometry is achieved. A small square patch of width s is etched at the center to connect all the arms. Finally, the outside of the four arms are detached from the metallic surface, and the four-arms star is completed.

Ref. [18] and [19] present the initial equations to design and determine the resonant frequency for the FSS using the four-arms star geometry. Based on this design procedure the FSS was designed to operate at 28 GHz. The dimensions of the structure are $p = 4.1$ mm, $a = 3.25$ mm, $s = 1.0$ mm and $b = 0.6$ mm, and considering a dielectric substrate with $\epsilon_r = 2.94$ and thickness of 0.508 mm.

B. FSS #2

The second geometry is based on a quasi-square shape, shown in Fig. 1b (FSS #2). To design it, initially a square patch p is dimensioned. Slot sections are inserted, crossing it in the middle, both vertically and horizontally, of width g_1 . In this part, the FSS behaves as a capacitor with a wideband response. The final step to achieve the geometry is to add a square slot of size g_2 in the center of the patch, and the metallic surface has a width of w . Depending on the size of this square, the FSS starts increasing its inductance and hence, its resonant frequency and bandwidth decrease.

This second FSS was designed for 36 GHz. The properties of the dielectric substrate and unit cell size ($p = 4.1$ mm) are the same as used in FSS #1. The design procedure is described in [19], and its dimensions are $w = 0.85$ mm, $g_1 = 0.2$ mm and $g_2 = 2.4$ mm.

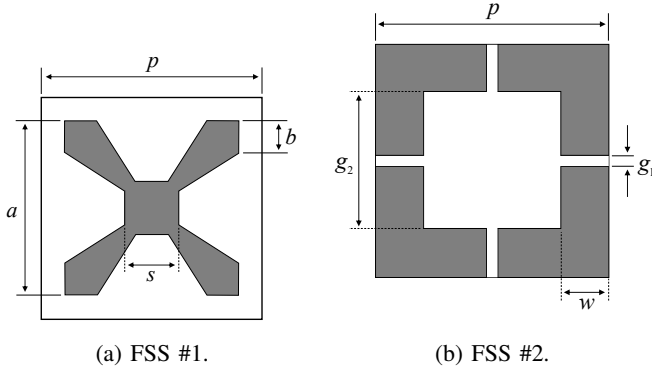


Fig. 1: Geometry and parameters of FSSs.

C. Cascaded FSSs

The cascading of the two FSSs is shown in Fig. 2. The coupling between the two structures is determined by their spatial separation d . Each single-layer structure provides a different transmission zero as discussed in Subsections II-A and II-B. The cascading was done considering an air gap of $d = 2.5$ mm [19].

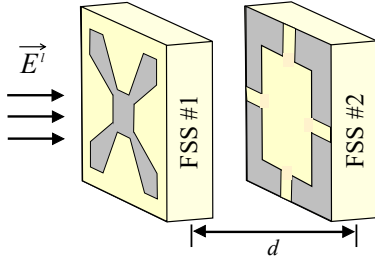


Fig. 2: Cascaded FSS structures.

The numerical results of the individual structures are used as a prediction in terms of frequency response of the cascaded FSS, considering a normal incidence wave, as shown in Fig. 3. The two resonant frequencies in the cascaded FSS are created by the resonators in each layer with values at 27.92 GHz and 36.04 GHz.

III. RESULTS

The numerical characterization was done considering the excitation of the proposed structure with the electric (E) field at transverse electric (TE), transverse magnetic (TM) incidence, and circular polarization, as shown in Fig. 4.

At normal incidence ($\theta = 0^\circ$), the E-field experiences a perfectly symmetrical structure in both (TE and TM) polarizations. When the wave is incident at an oblique angle ($\theta \neq 0^\circ$), the E-field starts to probe the broken intrinsic symmetry of the proposed structure, hence its frequency response changes. In this condition for the TE polarization, a sharp asymmetric line-shaped Fano resonant is excited when $\theta \geq 20^\circ$ (Fig. 5), due to the interference between the two independent resonance modes, as f_{z2} moves closer to f_{z1} . Fig. 5 shows that the profile of the FR is stable with an increase

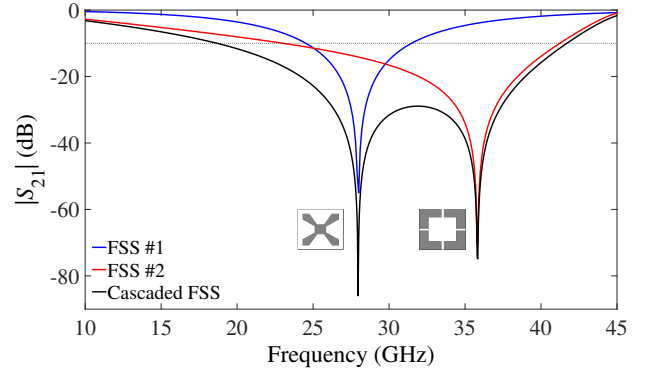


Fig. 3: Comparison of numerical results of individual FSSs and cascaded ones at normal incidence.

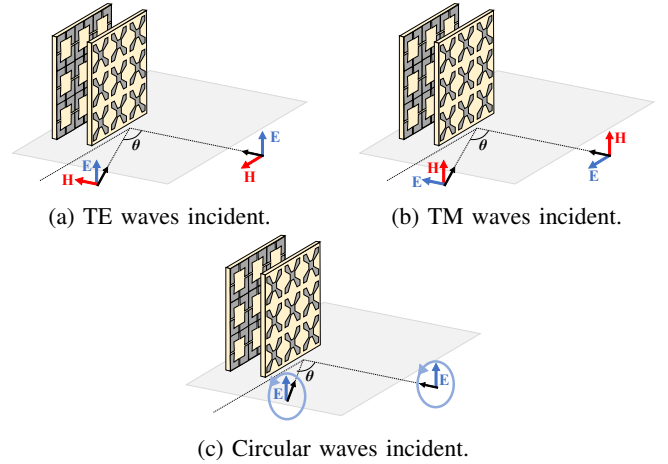


Fig. 4: Polarizations of the incident wave on the cascaded FSS.

of amplitude and bandwidth while increasing the angle of incidence.

To verify the FR response of the proposed structure, two FSSs were manufactured. The prototypes were fabricated on single-layer Rogers Duroid/RT 6002 dielectric substrate with $\epsilon_r = 2.94$, thickness of 0.508 mm, and loss tangent of 0.0012, with 26×26 elements and overall dimensions of 10.7 cm \times 10.7 cm (Fig. 6).

Measurements were carried out in an anechoic chamber, the prototype is placed in the stand between two directive antennas, where one acts as a transmitter (T_x) and the other as a receiver (R_x). The two horn antennas were placed facing each other at a fixed position, with a distance of 80 cm.

Fig. 7 shows the measured transmission coefficient along with numerical results for the proposed FSS for TE polarization at normal ($\theta = 0^\circ$) and oblique incidence ($\theta = 30^\circ$). The air gap between the structures is $d = 2.5$ mm, provided by using Teflon spacers, nuts and screws to complete the cascade. The measured transmission zeros at normal incidence are 28.08 GHz and 36 GHz, and show excellent agreement with those obtained by CST ($f_{z1} = 27.92$ GHz and $f_{z2} = 36.04$

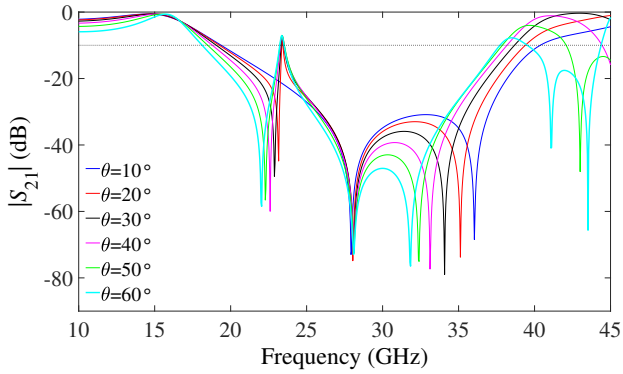


Fig. 5: Simulated results for the TE polarization of the cascaded FSS at different incident angle.

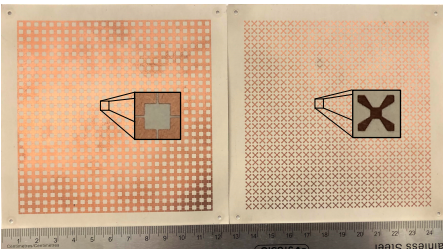


Fig. 6: Fabricated FSSs with quasi-square (left) and four-arms star (right) geometries, and their individual cells.

GHz). From numerical result, the cascaded FSS at normal incidence has a 10-dB return-loss bandwidth of 24.38 GHz, going from 18.34 to 42.72 GHz. Due to limitations in the frequency range of the horn antennas used, the measured results are shown from 21.5 GHz to just 40 GHz, although it can be observed that the experimental curve closely follows the numerical one. The measured and simulated results at $\theta = 30^\circ$ for f_{z1} are 28.11 GHz and 28.28 GHz, respectively. The resonance f_{z2} changed to a lower frequency, when compared to normal incidence, and it is found to be at 35.07 GHz (measured) and 34.24 GHz (CST). For this polarization, the structure is weakly coupled to free space, which leads to the emerge of FR at 23.3 GHz (measured) and 23.16 GHz (CST).

The characterization of the TM polarization was also performed numerically and experimentally (Fig. 8). At normal incidence, the structure is symmetric and the results obtained are very similar to the TE polarization, as expected. The first transmission zero is 28.02 GHz in measured results, and 27.96 GHz for the numerical one. The measured and simulated results of the second transmission zero are 36.17 GHz and 36.04 GHz, respectively. The numerical bandwidth is 24.36 GHz with a band-stop range from 18.34 GHz to 42.70 GHz. The transmission coefficient of simulated and measured results for off-normal incidence with $\theta = 30^\circ$ is analyzed. It is observed that the f_{z1} remains basically at the same frequency, but f_{z2} is moved to a higher frequency (37.08 GHz in CST and 37.13 GHz measured). This change occurs because the

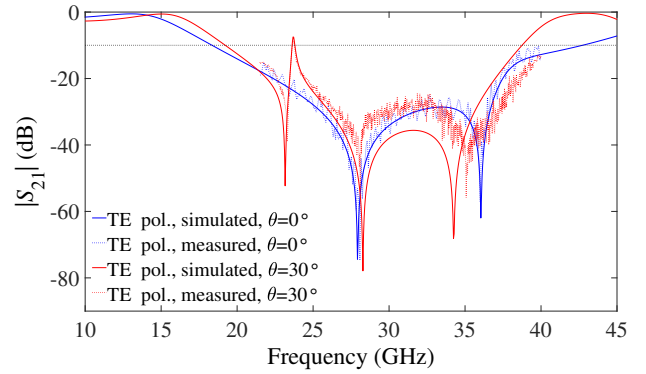


Fig. 7: Simulated and measured results for the TE polarization of the cascaded FSS at normal and oblique incidence.

dimensions of parameters w and g_1 of the FSS #2, seen by the wave with incidence at $\theta = 30^\circ$ for TM polarization, are reduced. The resonances of the proposed structure are coupled strongly to free space, thus not generating any Fano mode. The result obtained numerically shows that the proposed FSS presents a wide bandwidth of approximately 20.56 GHz.

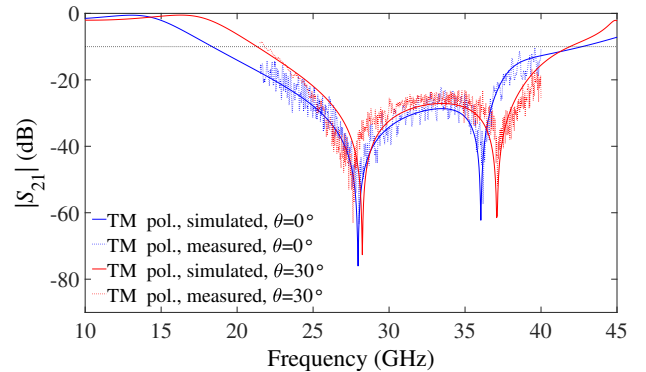


Fig. 8: Simulated and measured results for the TM polarization of the cascaded FSS at normal and oblique incidence.

By analyzing the influence of the parameters of FSS #1 and FSS #2 considering the case when $\theta = 30^\circ$ for TE polarization, the distortion of the transmissivity curve is found to happen when the size of the element of FSS #1 changes. This distortion is the dark mode (or FR), and the investigation of its response is presented in Fig. 9 for different values of a . With the change of this parameters, f_{z1} is also affected since it corresponds to the resonance of the resonator FSS #1. While a increases, the FR and f_{z1} are reduced as well as the FR amplitude. These results are summarized in Table I.

TABLE I: Resonant frequencies of FR and f_{z1} for different values of a .

a (mm)	3.00	3.25	3.50	3.75
FR (GHz)	25.54	23.16	20.57	18.15
f_{z1} (GHz)	30.19	28.28	26.06	24.00

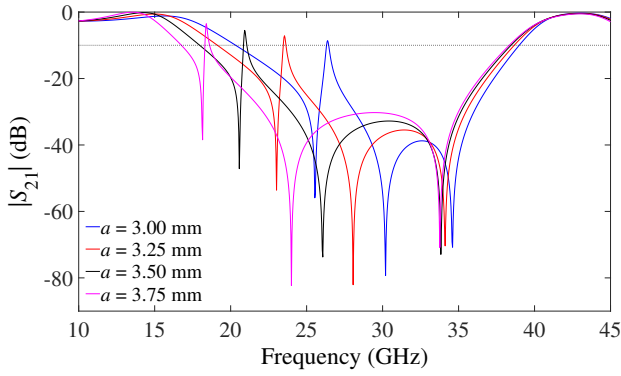


Fig. 9: Influence of FSS #1 on the Fano resonance, with dimensions dimensions $p = 4.1$ mm, $b = 4.1$ mm and $s = 1.0$ mm, and substrate permittivity $\epsilon_r = 2.94$ and 0.508 mm thickness, at $\theta = 30^\circ$.

An incoming circular polarized wave arrives on the cascaded FSS at $\theta = 30^\circ$ as illustrated in Fig. 4c, and the result of the axial ratio (AR) of the transmitted wave is presented in Fig. 10. The maximum AR is found at the Fano resonance, proving that the vertical and horizontal components are affected differently, resulting in an outgoing elliptically polarized wave.

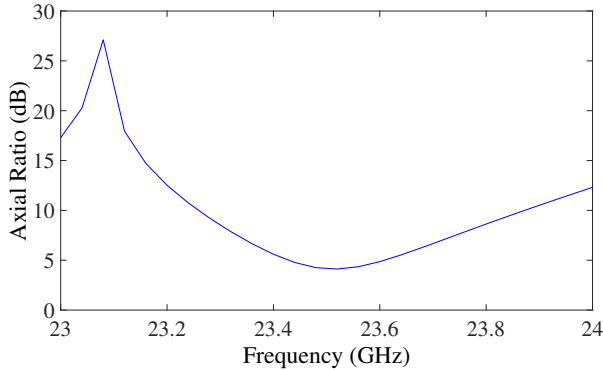


Fig. 10: Simulated axial ratio of the proposed structure.

IV. CONCLUSION

A symmetric double-layer FSS is proposed in this paper, and the Fano effects are demonstrated in the millimeter-wave range. The FR emerges when the proposed structure experiences off-normal incidence with $\theta = 20^\circ$ for TE polarization, and then its symmetry is broken. The occurrence of the FR was confirmed through numerical and experimental characterization. The Fano mode was only present in the TE polarization, showing that the proposed structure is polarization selective. The influence of the element size of FSS #1 in generating the FR was investigated.

REFERENCES

[1] B. A. Munk, "Element types: a comparison," in *Frequency Selective Surfaces: Theory and Design*. Wiley, 2000, pp. 50–51.

[2] R. S. Anwar, L. Mao, and H. Ning, "Frequency selective surfaces: A review," *Applied Sciences*, vol. 8, no. 9, p. 1689, 2018.

[3] A. A. Omar and Z. Shen, "Thin 3-D bandpass frequency-selective structure based on folded substrate for conformal radome applications," *IEEE Transactions on Antennas and Propagation*, vol. 67, no. 1, pp. 282–290, 2019.

[4] D. F. Mamedes and J. Bornemann, "High-gain reconfigurable antenna system using pin-diode-switched frequency selective surfaces for 3.5 GHz 5G application," in *Proc. SBMO/IEEE MTT-S International Microwave and Optoelectronics Conference (IMOC)*, 2021, pp. 1–3.

[5] B. Li, Y.-S. Zeng, B.-J. Chen, and C. H. Chan, "Terahertz frequency-selective surface with polarization selection and conversion characteristics," *IEEE Transactions on Terahertz Science and Technology*, vol. 9, no. 5, pp. 510–519, 2019.

[6] M. Pazokian, N. Komjani, and M. Karimipour, "Broadband RCS reduction of microstrip antenna using coding frequency selective surface," *IEEE Antennas and Wireless Propagation Letters*, vol. 17, no. 8, pp. 1382–1385, 2018.

[7] M. Mahmoodi, L. VanZant, and K. M. Donnell, "An aperture efficiency approach for optimization of FSS-based sensor resolution," *IEEE Transactions on Instrumentation and Measurement*, vol. 69, no. 10, pp. 7837–7845, 2020.

[8] B. Luk'Yanchuk, N. I. Zheludev, S. A. Maier, N. J. Halas, P. Nordlander, H. Giessen, and C. T. Chong, "The Fano resonance in plasmonic nanostructures and metamaterials," *Nature Materials*, vol. 9, no. 9, pp. 707–715, 2010.

[9] K. Karthigeyan, E. Manikandan, E. Papanasam, S. Radha, and B. Sreeja, "Multiband Fano resonance in symmetry broken planar terahertz metamaterial," in *Proc. Int. Conf. Devices for Integrated Circuit (DevIC)*, 2021, pp. 1–3.

[10] C. Wu, N. Arju, G. Kelp, J. A. Fan, J. Dominguez, E. Gonzales, E. Tutuc, I. Brener, and G. Shvets, "Spectrally selective chiral silicon metasurfaces based on infrared Fano resonances," *Nature Communications*, vol. 5, no. 1, pp. 1–9, 2014.

[11] X. Guo, H. Hu, X. Zhu, X. Yang, and Q. Dai, "Higher order Fano graphene metamaterials for nanoscale optical sensing," *Nanoscale*, vol. 9, no. 39, pp. 14 998–15 004, 2017.

[12] M. F. Limonov, M. V. Rybin, A. N. Poddubny, and Y. S. Kivshar, "Fano resonances in photonics," *Nature Photonics*, vol. 11, no. 9, pp. 543–554, 2017.

[13] C. Debus and P. H. Bolivar, "Frequency selective surfaces for high sensitivity terahertz sensing," *Applied Physics Letters*, vol. 91, no. 18, p. 184102, 2007.

[14] A. Yang, T. B. Hoang, M. Dridi, C. Deeb, M. H. Mikkelsen, G. C. Schatz, and T. W. Odom, "Real-time tunable lasing from plasmonic nanocavity arrays," *Nature Communications*, vol. 6, no. 1, pp. 1–7, 2015.

[15] M. Amin, R. Ramzan, and O. Siddiqui, "Fano resonance based ultra high-contrast electromagnetic switch," *Applied Physics Letters*, vol. 110, no. 18, p. 181904, 2017.

[16] J. He, J. Wang, P. Ding, C. Fan, and E. Liang, "Gain-assisted plasmon induced transparency in T-shaped metamaterials for slow light," *Journal of Optics*, vol. 17, no. 5, p. 055002, 2015.

[17] B. Luk'Yanchuk, N. I. Zheludev, S. A. Maier, N. J. Halas, P. Nordlander, H. Giessen, and C. T. Chong, "The Fano resonance in plasmonic nanostructures and metamaterials," *Nature Materials*, vol. 9, no. 9, pp. 707–715, 2010.

[18] D. F. Mamedes, J. Bornemann, and A. G. Neto, "Linear-to-circular polarization converter based on four-arms star FSS at 5.2 GHz for 5G applications," in *Proc. 16th European Conference on Antennas and Propagation (EuCAP)*, 2022, pp. 1–4.

[19] D. F. Mamedes and J. Bornemann, "Using an equivalent-circuit model to design ultra-wide band-stop frequency-selective surface for 5G mm-wave applications," *IEEE Open Journal of Antennas and Propagation*, vol. 3, pp. 948–957, 2022.